Complicated synergistic effects between three corrosion inhibitors for Q235 steel in a CO₂-saturated 3.5 wt% NaCl solution

Junlei Tang[1], Yuxin Hu[1], Hu Wang[2,*], Yuanqiang Zhu[1], Yuan Wang[1], Zhen Nie[3], Yingying Wang[1], Bernard Normand[4]

[1] School of Chemistry and Chemical Engineering, Southwest Petroleum University, Chengdu 610500, China
[2] School of Material Science and Engineering, Southwest Petroleum University, Chengdu 610500, China
[3] Research Institute of Petroleum Exploration and Development, CNPC, Beijing 100083, China
[4] Université de Lyon, INSA Lyon, MATEIS UMR CNRS 5510, Bat L. de Vinci, 21 Avenue Jean Capelle, 69621 Villeurbanne cedex, France
[*]E-mail: senty78@126.com

The corrosion inhibition of a one-component inhibitor, a bicomponent inhibitors and a three-component inhibitor consisting of 4-methylpyridine quaternary ammonium salt (PQ), quinoline quaternary ammonium salt (QQ) and thiourea (TU) for Q235 steel in a CO₂-saturated 3.5 wt% NaCl solution was investigated by electrochemical measurements, XPS analysis and quantum computational chemistry. The results showed that there were remarkable synergistic effects between PQ, QQ and TU, especially in the three-component inhibitor PQ+QQ+TU (1.5:1.5:1). It was also indicated that the different addition sequences of the three inhibitors had a significant influence on the synergistic effect. Additionally, the mechanism of the synergistic effects within the three-component inhibitor was proposed.

1. INTRODUCTION

Severe CO₂ corrosion of carbon steel often occurs in oil and natural gas exploitation, processing and transportation. Dissolved CO₂ in the produced water decreases the pH value and then induces harsh acid corrosion [1–3]. Due to the low-cost and ease of operation, injection of inhibitor is one of the most effective measures for the protection of CO₂ corrosion in the petroleum industry [4–6].

Currently, organic corrosion inhibitors are widely used in real application, most of which contain unsaturated bonds and atoms, such as N, S, O and P. Such inhibitor forms an adsorption film, in most occasion, on the metal surface to expel the corrosive medium, in which the adsorption action relies on the lone pair electrons of the organic inhibitor to form covalent bonds with the orbitals of the metal atoms [7]. Imidazole, quinoline, pyridine and their derivatives are most commonly used to control CO_2 corrosion owing to the structure of the nitrogen-containing heterocycle.

Imidazoline and its derivatives have been widely studied in the lab and in real application. The drawbacks are their relative instability in storage, emulsifying tendency in produced water and relatively expensive in economy [8,9]. Quinoline and its derivatives have also been widely studied and used. The excellent inhibition performance and water solubility enhance the application [10–13]. Pyridine molecules contain an N atom and a heterocyclic group. It has been proven to have excellent corrosion inhibition performance in a strong acid environment [14]. However, it has rarely been studied in a CO_2 environment. Several researchers have discovered that these compounds adsorb in parallel on iron-based metal surfaces by the action of the nitrogen-containing heterocycle [15,16]. In addition, distinct functional groups and molecular structures have a great influence on the corrosion inhibition performance [17,18].

It is also worth mentioning that synergistic inhibition effects exist, in which the performance of mixed inhibitors is better than that of individual inhibitor on the corrosion of metals. This has been proven to be an effective means of improving the efficiency of the inhibitors, decreasing the amount of inhibitor usage and applying in a variety of aggressive media of complex environments [19,20]. The synergistic effects are far more ahead in practical applications than in laboratory research. Moreover, a large majority of research works on the synergistic effects of two kinds of corrosion inhibitors is based on the type, content ratio and concentration to explore the synergistic mechanism [21–25]. However, the synergistic effects of three-component inhibitors and the influence of the adding sequence on the performance of three-component inhibitors have rarely been reported.

In this study, 4-methylpyridine quaternary ammonium salt (PQ) and quinoline quaternary ammonium salt (QQ) were synthesized and used as corrosion inhibitors. Thiourea (TU) was also used as a corrosion inhibitor alone or combined with the other inhibitors. The synergistic effects of the three inhibitors at different molar ratios in a CO_2-saturated 3.5 wt% NaCl solution for carbon steel were studied by potentiodynamic polarization and electrochemical impedance spectroscope (EIS). X-ray photoelectron spectroscopy (XPS) measurements and quantum chemical calculations were carried out to analyze the synergistic adsorption of the inhibitors. The competitive adsorption mechanism was discussed as well.
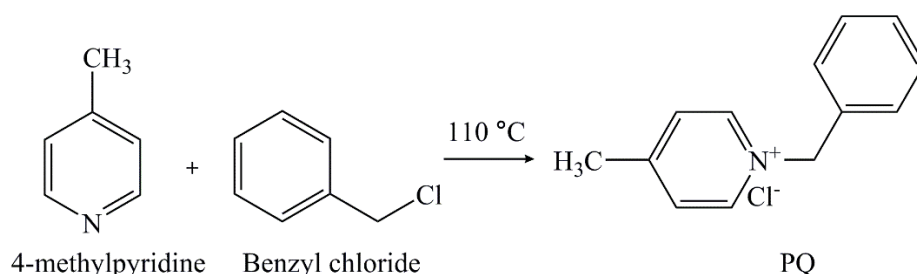
2. EXPERIMENTAL

2.1 Materials

The molecular structures of TU, PQ and QQ are shown in Figure 1. PQ and QQ were synthesized by reacting 4-methylpyridine and quinoline with benzyl chloride at 110°C for 4 hours, followed by recrystallization with ethanol, respectively. The synthesis method is shown in Figure 2.
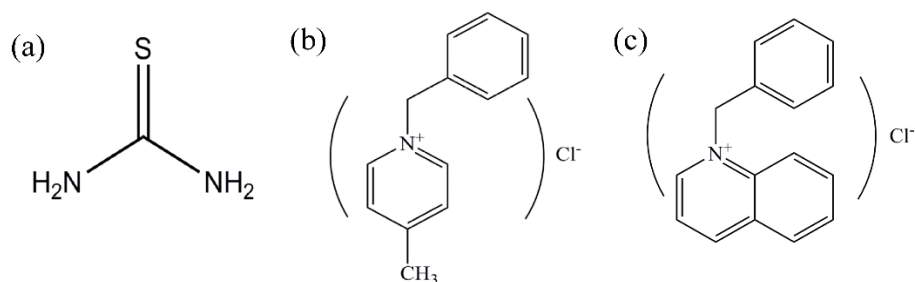
Figure 1. Molecular structures of (a) TU, (b) PQ and (c) QQ.

Figure 2. Chemical reaction process of quaternization.

The specimen used in this study was Q235 steel with the following composition (wt %): C 0.16, Si 0.30, Mn 0.53, P 0.015, S 0.004 and Fe balance. The corrosion medium was 3.5 wt% NaCl solution. The deaeration procedure was carried out before the experiment. Nitrogen gas was continuously purged into the solution for 2 hours and then, the solution was saturated at atmospheric pressure by continuous purging with carbon dioxide gas for 0.5 hours. During the electrochemical measurements, CO_2 gas was continuously bubbled. All the experiments were conducted at $60 \pm 1°C$.

2.2. Electrochemical experiments

All the electrochemical tests were carried out on a *Corr Test* electrochemical workstation (Wuhan Corrtest Instruments Co. Ltd. CS350). The data were processed by the software CorrTest (Ver 4.5). A conventional three electrodes system was carried out in a glass cell containing 100 ml of the corrosive medium solution. The working electrode (WE) was an L type cylindrical electrode wrapped in Teflon through the machine processing and the exposed test area was 0.5 cm^2. The saturated calomel electrode (SCE) was used as the reference electrode (RE). A platinum plate with a surface area of 1 cm^2 was used as the counter electrode (CE). Before each experiment, the work electrode was polished by sandpaper (grade 500, 1000, 2000, respectively) and dried with a cold drier after rinsing with deionized water and alcohol.

Potentiodynamic polarization curves were conducted with a potential range from –400 mV to +400 mV (vs. OCP) at a scan rate of 0.5 mV s^{-1} when the open circuit potential (OCP) was in a steady state after immersing in corrosion media for 2 hours, both in the presence and absence of corrosion inhibitor. The inhibition efficiency (*IE%*) was calculated from the polarization curves by means of the following equation:

$$IE\% = \frac{i_{\text{corr}(0)} - i_{\text{corr}(\text{inh})}}{i_{\text{corr}(0)}} \times 100 \qquad (1)$$

where $i_{\text{corr}(0)}$ represents the corrosion current density in the absence of inhibitor, and $i_{\text{corr}(\text{inh})}$ stands for corrosion current density in the presence of inhibitor. On account of the influence of the different adsorption order of the inhibitors on the metal surface, the adding order of each inhibitor during the immersion period was designed. Hence OCP measurement and EIS were carried out to investigate the synergistic behavior of the inhibitors. The OCP measurement was conducted to record the variation of the potential with and without inhibitor for 90 minutes, including the addition of PQ, QQ, and TU respectively at every 30 minutes. In addition, impedance measurements were performed over the frequency range from 0.01 Hz to 100 kHz at stable OCP with 10 mV AC amplitude at different immersion time. The number of frequency points was reduced in order to guarantee that the EIS measurement can be completed within approximately 10 minutes. Moreover, polarization resistance tests were performed individually on the same electrode under a potential range from –10 mV to +10 mV (vs. OCP) at a scanning rate of 0.2 mV s^{-1} every 10 minutes which took approximately 1 minute and the test condition was the same as that of EIS.

2.3. Surface analysis

The XPS spectra from an XPS XSAM800 with Al Kα as the excitation source were used to analyze the film formed on the specimen. The entire-range (200 eV) XPS scan was performed on the specimens first, followed by a narrow-range (20~30 eV) scan of the specified elements during the test. The values of the binding energies were calibrated against C 1s at 284.5 eV. The carbon steel specimens were immersed in CO_2-saturated 3.5 wt% NaCl solution for 90min with the addition of PQ, QQ and TU simultaneously and separately at different addition order, in which a total concentration was 5×10^{-5} mol/L with a 1.5:1.5:1 molar ratio at 60°C. The specimens were washed by deionized water, dried with a cold drier and then tested by XPS.

2.4. Quantum chemical study

The M06-2x hybrid functional method was used to optimize the geometric structure of the inhibitor and calculate the quantum chemical parameters through the Gaussian 09 software package. The relevant quantum chemical parameters including the energies of LUMO (E_{LUMO}), HOMO (E_{HOMO}) and energy gap (ΔE) for the three inhibitors were considered [26].

3. RESULTS AND DISCUSSION

3.1. Potentiodynamic polarization tests

Potentiodynamic polarization tests of Q235 in CO_2-saturated 3.5 wt% NaCl solution at 60°C were carried out in the absence and presence of different kinds of corrosion inhibitors. The tested corrosion inhibitors include PQ, QQ and TU with the total concentration of 5×10^{-5} mol/L, regardless of whether they are used alone or as a mixture of inhibitors. The molar ratios of the mixed inhibitors were

fixed at 3:1 (heterocyclic big molecule: small molecule) which showed better inhibition performance based on the preliminary experimental results. The results of polarization curves are shown in Figure 3. Table 1 is the corresponding parameters obtained from fitting of polarization curves.

It is shown in Figure 3 that all the curves exhibit a similar shape, indicating very a close mechanism in nature. The anodic process is controlled by activation dissolution and no apparent passivation can be observed on the curves [27,28]. With the addition of the corrosion inhibitors, the curves move toward the left on the plane coordinates. The corrosion potential shifts slightly with the presence of corrosion inhibitors.

The polarization curve only changes a little with the presence of individual inhibitors, at a concentration of 5×10^{-5} mol/L. The inhibition efficiency is not very high for all three inhibitors. Especially for PQ and TU, both of them are not useful or only slightly effective in inhibiting corrosion process. When judging from the electrochemical parameters, the presence of TU has an inhibition effect on the cathodic process, and the cathodic Tefel constant, $-b_c$, varies from 414.3 mV (blank solution) to 593.2 mV, indicating that TU adsorbs on the cathode preferentially. The presence of QQ induces the variation of b_a and b_c slightly. However, the corrosion current density decreases remarkably and the inhibition efficiency mounts to 51.2%. It is clear that QQ is a mixed type corrosion inhibitor which influences both the cathodic and anodic processes of corrosion.

For bicomponent inhibitors, in the presence of PQ+TU (molar ratio of 3:1 and total concentration of 5×10^{-5} mol/L), QQ+TU (3:1) and PQ+QQ (1:1), the inhibition efficiency notably increases. There are apparent synergistic effects between the inhibitors in the presence of bicomponent inhibitors. Although the total amount of the added inhibitor is constant, an elevated corrosion inhibition is observed compared to adding a one-component inhibitor alone. It implies that the synergism between two inhibitors enhances the inhibition effects. The best inhibition efficiency is observed for at PQ+QQ (1:1).

The corrosion inhibition efficiency is further increased with the addition of a three-component inhibitor. As seen in the figure, the curve in the presence of the three-component inhibitor is located at the far left, indicating that the corrosion process has remarkably decreased. It is shown in Table 1 that after the addition of the three-component inhibitor both the cathodic and anodic processes are influenced.
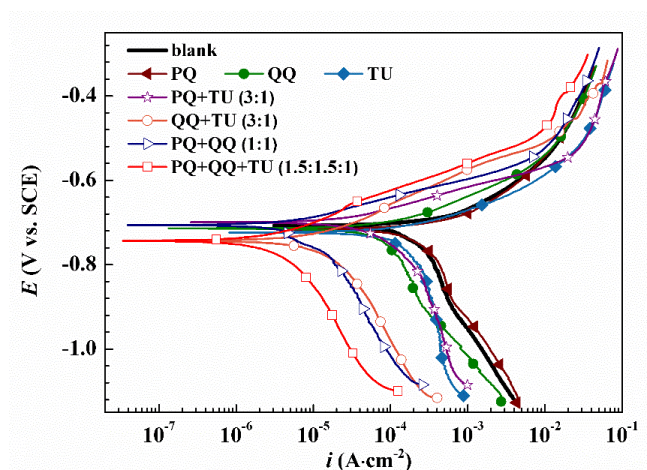
Figure 3. Potentiodynamic polarization curves for Q235 steel in CO_2-saturated 3.5 wt% NaCl solution in the absence and presence of different corrosion inhibitors (total concentration of 5×10^{-5} mol/L) at 60°C.

Table 1. Potentiodynamic polarization parameters and inhibition efficiencies for Q235 steel in CO_2-saturated 3.5 wt% NaCl solution in the absence and presence of different corrosion inhibitors (total concentration of 5×10^{-5} mol/L) at 60°C.

Inhibitor	E_{corr} vs. SCE (V)	b_a (mV)	$-b_c$ (mV)	i_{corr} (μA cm^{-2})	IE%
Blank	-0.708	52.4	414.3	214.3	-
PQ	-0.716	53.3	413.1	256.6	-19.7
QQ	-0.714	86.2	382.9	104.6	51.2
TU	-0.724	67.7	593.2	180.6	15.7
PQ+TU (3:1)	-0.699	59.0	547.2	42.2	80.3
QQ+TU (3:1)	-0.743	91.5	255.3	23.1	89.2
PQ+QQ (1:1)	-0.706	60.1	372.7	18.4	91.4
PQ+QQ+TU (1.5:1.5:1)	-0.744	82.6	327.9	9.4	95.6

3.2. Synergistic mechanism of competitive adsorption

3.2.1. OCP variations at different conditions

To obtain the competitive adsorption behavior and synergistic mechanism of the inhibitors on the Q235 steel surface, OCP monitoring was carried out by adding corrosion inhibitors at different immersion times in sequence. Figure 4 compares the variations of OCP with time, in which different corrosion inhibitors are added with different sequences at a specific time during the monitoring process. In all three graphs, curve 4 is the blank solution without adding any inhibitor and curve 1 is the one with the three-component inhibitor added at the beginning of immersion. In blank solution, OCP moves negatively. Then a relatively stable OCP state is established with prolonged immersion time. That is, because of the relatively close rates of the corrosion process and formation of oxides at the interface. In curve 1, OCP moves towards the positive direction rapidly, and then it declines and stabilizes very slowly. The different behaviors can be attributed to the opposite processes existing at the metal/solution interface in the presence of the three-component inhibitor [29]. On one hand, the inhibitors form a protective film on the metal surface, which leads to the shift of the OCP value to the positive direction. On the other hand, the metal corrodes in the medium, which results in a decrease of the potential. It is also noticed that, the initial OCP of the three-component inhibitor is much more noble than in the blank solution, implying a more thermodynamically stable state. This can be explained as the result of the effective adsorption of inhibitor molecules on the metal surface [30].
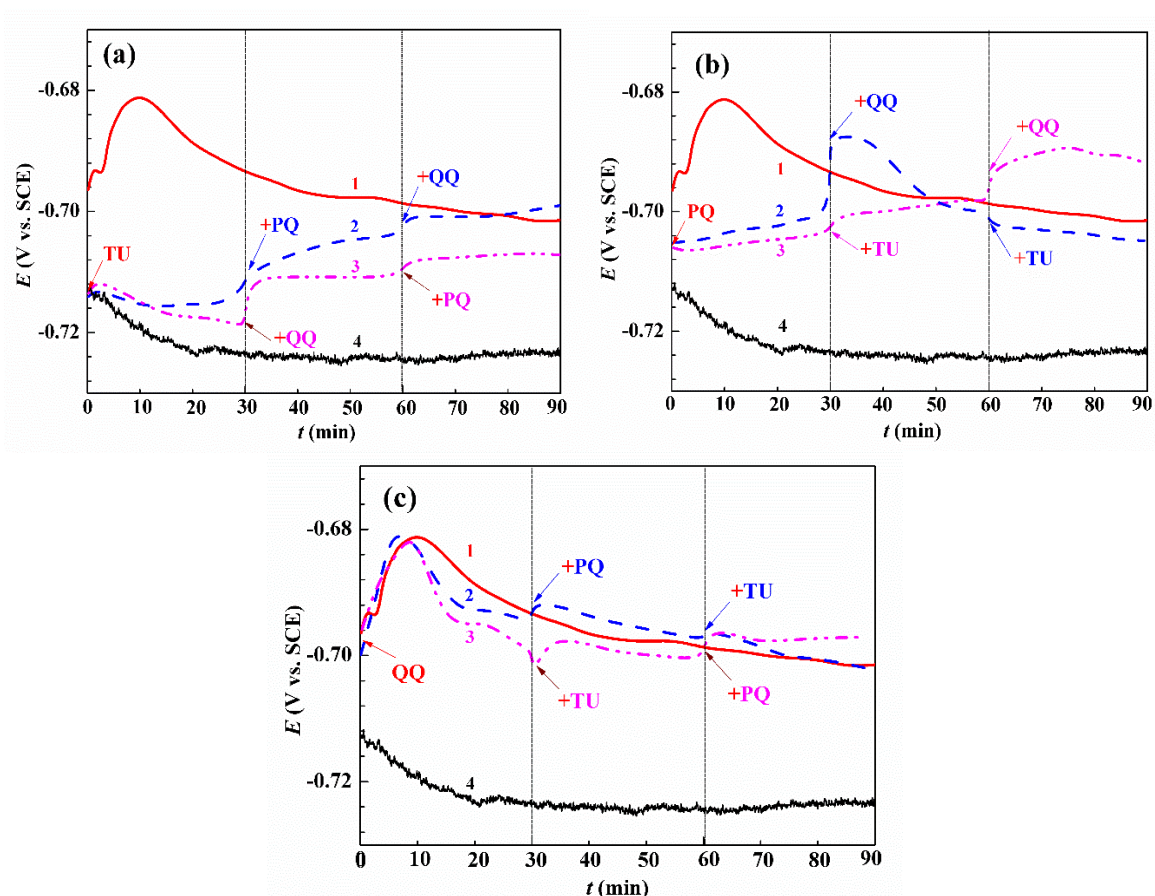
Figure 4. OCP variations with time in the different adding sequences of inhibitors. Curve 1 in all the graphs stands for adding mixture inhibitor (5×10^{-5} mol of total amount with molar ratio of PQ:QQ:TU=1.5:1.5:1) at the beginning of OCP monitoring. Curve 4 in all the graphs represents OCP in the absence of inhibitor. Curve 2 and 3 refer to different adding sequences in OCP monitoring (a) TU added at the beginning, (b) PQ added at the beginning and (c) QQ added at the beginning.

In Figure 4(a), TU had been added preferentially at the beginning of OCP monitoring (curve 2 and 3). It shows that OCP gradually moves negatively in the presence of TU. In curve 2, PQ was added at t=30 min and QQ at t=60 min. It is demonstrated that in both curves the addition of QQ and PQ leads to the positive shift of OCP, indicating the apparent influence of PQ and QQ in the presence of TU. However, no remarkable or intrinsic difference can be obtained from the sequence of adding PQ and QQ. Figure 4(b) compares the condition of adding PQ preferentially. It is shown in curves 2 and 3 of Figure 4(b) that the initial potential at this condition is more positive than blank and adding TU preferentially, although not as noble as adding the three-component inhibitor. The adding sequence of TU and QQ has a pronounced influence on the OCP variation. In curve 2, QQ was added at t=30 min and then TU was added at t=60 min. It presents that the addition of QQ results in a very steep increase in the potential and then it decreases slowly. The presence of TU only induces slight fluctuation of the potential. Curve 3 displays a different behavior. The presence of TU at t=30 min only leads to a slight increase in the potential, while the presence of QQ at 60 min causes a prominent ascent in the potential. The comparison reveals that QQ has a more notable influence than TU. In Figure 4(c), QQ had been added preferentially at 0 minute, as shown in curves 2 and 3. It is shown that under this circumstance,

the OCP variations are very close to the condition of adding three-component inhibitor preferentially. The later addition of TU or PQ only changes the behavior slightly. Additionally, PQ has a more positive influence than TU. By comparison with all the curves in Figure 3, it is evident that the influence orders of the three inhibitors are as follows: QQ > PQ > TU.

3.2.2. Polarization resistance measurements

The polarization resistances (R_p) of adding three inhibitors at the same time and in different orders are shown in Figure 5. In all three figures, adding the mixture of inhibitors (three-component inhibitor, TU+PQ+QQ) at t=0 min is presented for comparison. It is shown that by adding the mixture inhibitors that R_p rises rapidly with immersion time and then stabilizes after 30 minutes, indicating that the fast process of film-forming completes within approximately 30 minutes. It can also be observed that the R_p values stabilize at a high value. The high value of R_p implies a low corrosion rate. Hence, it can be concluded that adding the mixture of inhibitors is very efficient in forming a protective film on the metal surface.
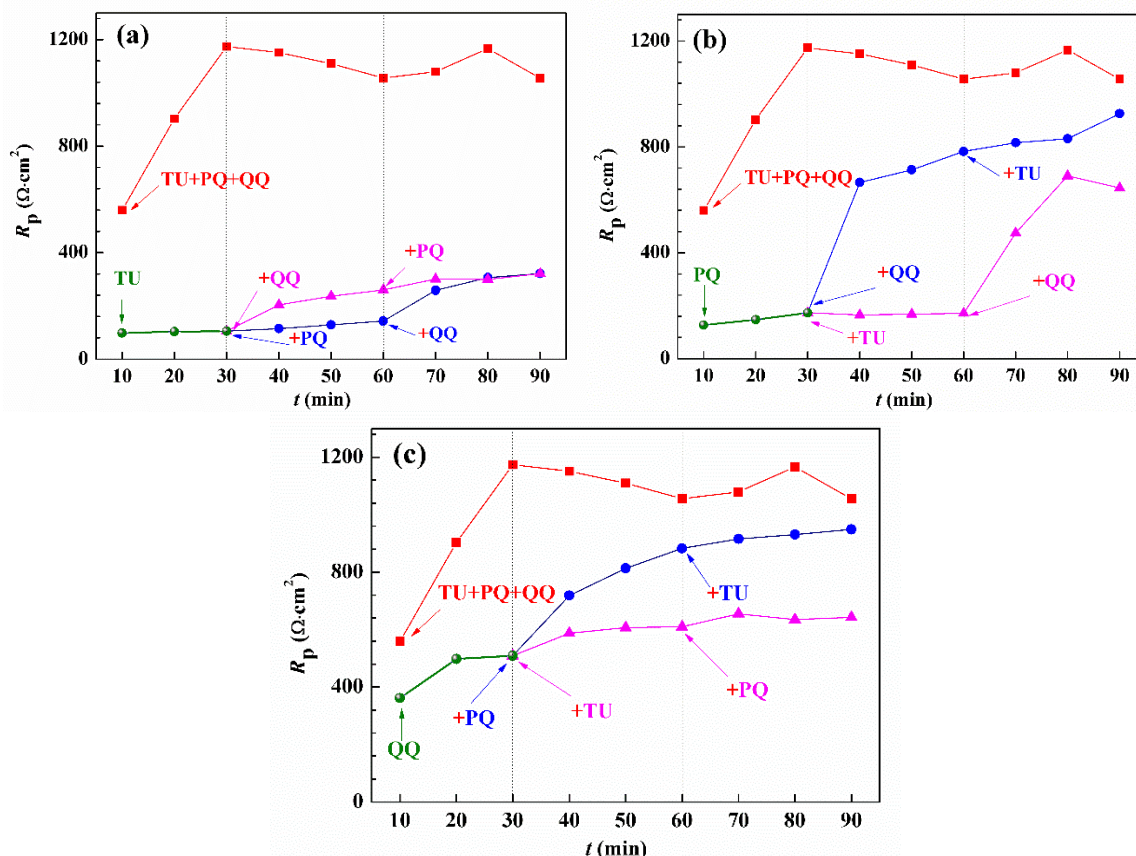
Figure 5. The variations of R_p with time, obtained by linear polarization with time for Q235 steel in CO$_2$-saturated 3.5 wt% NaCl solution at 60°C with adding mixture inhibitors (1.875×10^{-5} mol / L PQ+1.875×10^{-5} mol / L QQ+1.25×10^{-5} mol / L TU) at the beginning and in different adding order for fixed molar ratio (a) adding 1.25×10^{-5} mol/L TU firstly, (b) adding 1.875×10^{-5} mol/L PQ firstly, (c) adding 1.875×10^{-5} mol/L QQ firstly.

Figure 5(a-c) compares the variations of R_p with immersion time under different inhibitor adding ways. For example, in Figure 5(a), TU was added at t=0 min. Then PQ or QQ was added at t=30 min. In

the end, QQ or PQ was added at t=60 min. The R_p value was measured at every ten minutes. The synergistic effects in different adding orders can be recognized by the R_p variations. It can be seen from the three figures that when adding different one-component inhibitors at t=0 min, R_p varies differently. QQ starts with a high R_p value and rises with prolonged time, indicating the best in efficiency which is in accordance with the polarization behavior and EIS (in 3.2.3). It also shows in Figure 5(a) that adding TU at t=0 min leads to poor synergistic effects, regardless of the orders of the later addition of PQ and QQ. It indicates that the film of TU on the metal surface is not very protective. Additionally, the film prevents the more protective film formed by PQ and QQ. In Figures 5(b) and 5(c), the subsequent addition of TU causes little variation in R_p. However, apparent synergistic effects happen between PQ and QQ. Regardless of how the adding orders change, the R_p value always rises sharply when adding another inhibitor of PQ or QQ. Additional discussion on the about synergistic effects of the three inhibitors will be carried out in the EIS measurements.

3.2.3 EIS measurements

EIS measurements were carried out by adding different corrosion inhibitors at different time intervals. Figures 6-8 compares the influence of the adding sequences of inhibitors on the EIS patterns. It is observed that the Nyquist plots display one capacitive loop in the blank solution, which implies the traditional and simplest electrochemical process. It can be explained by the equivalent circuit diagram in Figure 9(a). The diameter of the semicircle markedly increases with the presence of corrosion inhibitors in comparison with the blank solution, suggesting that the addition of inhibitors can effectively retard the electrochemical corrosion of Q235 steel in CO_2 solution. Curves 1, 2 and 3, in the three figures, respectively, are all under the condition of adding the mixture inhibitors of PQ, QQ and TU (three-component inhibitor). The difference between curves 1, 2 and 3 lies in the immersion time before EIS measurement. Curve 1, 2 and 3 are measured in the presence of the three-component inhibitor with different immersion times: 30 min for curve 1, 60 min for curve 2 and 90 min for curve 3. It is apparent that the capacitive loops of curves 1, 2 and 3 are much bigger than others, indicating that a more efficient protective film is formed on the steel surface.

Figure 6 reveals the different EIS patterns of the three inhibitors, PQ, QQ and TU, used as one-component inhibitors. It is shown that in the presence of different inhibitors, it behaves differently. Although it is far smaller than curve 1, the diameter of the capacitive loop of QQ is much larger than that of TU and PQ. It indicates that QQ is very effective in adsorbing on the metal surface to retard the corrosion process. It also implies that QQ and TU are both not very effective when used alone. Additionally, in the presence of PQ, it shows two time constants. The higher frequency capacitive loop can be related to the capacitance and resistance of the adsorbed PQ film on the metal surface, and the lower one can be attributed to the Faraday charge transfer process at the metal surface.

Figure 7 shows the influence of the adding sequences of bicomponent inhibitors on the EIS behavior. When adding two inhibitors, named as bicomponent inhibitors, the adding sequence can possibly have a remarkable influence on the inhibition performance. A symbol such as [1]TU[2]PQ represents adding TU at the beginning of immersion, adding PQ after 30 min of immersion and conducting the EIS test at t=60 min. It can be seen from the Nyquist plot that in the presence of [1]TU[2]PQ,

the diameter of the capacitive loop has a limited increment. The size order of the capacitive loop is as follows: $^1QQ^2PQ > {}^1QQ^2TU > {}^1PQ^2QQ > {}^1TU^2QQ > {}^1PQ^2TU > {}^1TU^2PQ$. It also indicates that adding QQ preferentially would be more efficient in forming protective film for bicomponent inhibitors.
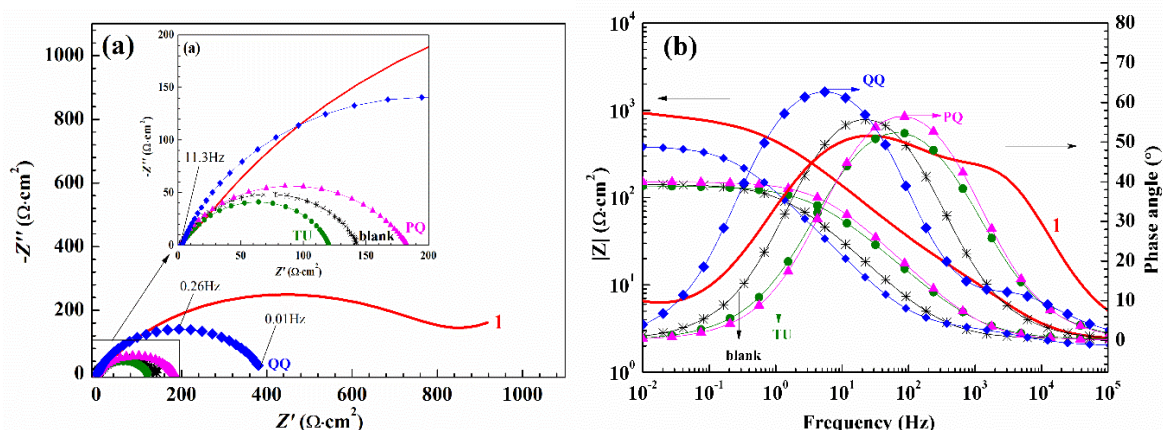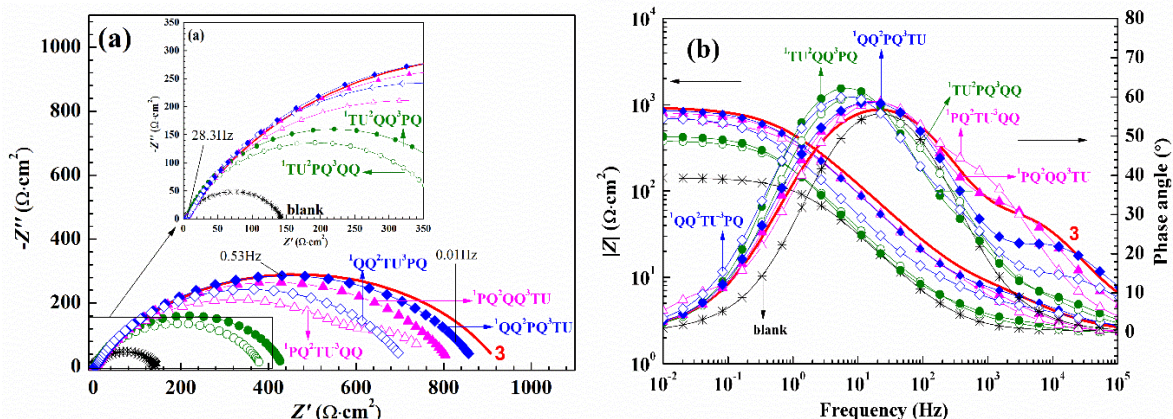

Figure 6. Nyquist (a) and Bode (b) plots for Q235 steel in CO_2-saturated 3.5 wt% NaCl solution at 60°C with no inhibitor (✳), adding mixture inhibitor (1.875×10^{-5} mol/L PQ+1.875×10^{-5} mol/L QQ+1.25×10^{-5} mol/L TU) initially and measuring EIS after immersing for 30 minutes (curve 1), adding one inhibitor separately at t=0 min and lasting for 30 minutes before measurement, labeled as 1.25×10^{-5} mol/L TU (●),1.875×10^{-5} mol/L PQ (▲) and 1.875×10^{-5} mol/L QQ (◆).
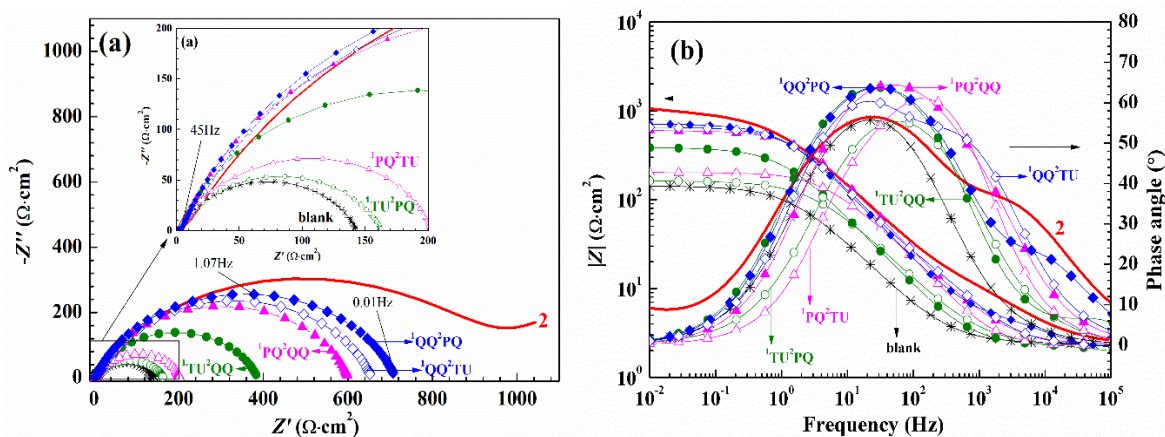
Figure 7. Nyquist (a) and Bode (b) plots of Q235 steel in CO_2-saturated 3.5 wt% NaCl solution at 60°C with no inhibitor (✳), adding mixture inhibitor (1.875×10^{-5} mol/L PQ+1.875×10^{-5} mol/L QQ+1.25×10^{-5} mol/L TU) initially and measuring EIS after immersing for 60 minutes (curve 2), adding bi-component inhibitors separately, labeled as $^1TU^2QQ$ (○), $^1TU^2PQ$ (●), $^1PQ^2TU$ (△), $^1PQ^2QQ$ (▲), $^1QQ^2TU$ (◇) and $^1QQ^2PQ$ (◆), in which 1and 2 represent the order of addition at t=0 min and 30 min by fixed molar ratio and testing after 30 and 60 minutes).

The EIS patterns of adding three inhibitors at different times are shown in Figure 8. It is obvious that the adding sequence has a remarkable influence on electrochemical behaivor. The largest capacitive loop occurs in $^1QQ^2PQ^3TU$. The size order of the capacitive loop is as follows: $^1QQ^2PQ^3TU > {}^1PQ^2QQ^3TU > {}^1QQ^2TU^3PQ > {}^1PQ^2TU^3QQ > {}^1TU^2QQ {}^3PQ > {}^1TU^2PQ^3QQ$. It further proves that QQ is more efficient than PQ and TU. Adding TU preferentially has the worst efficiency. However, TU also has a positive contribution to the synergism in the three-component inhibitor, which can be concluded by comparing the capacitive loops of the bicomponent inhibitors (Figure 7a) and three-component

inhibitor (Figure 8a). The Bode plots of Figure 8(b) also show that two capacitive loops can be observed. The capacitive loop at higher frequency is very apparent when adding QQ or PQ preferentially, while adding TU preferentially, the capacitive loop at higher frequency is not quite clear.

Figure 8. Nyquist (a) and Bode (b) plots of Q235 steel in CO_2-saturated 3.5 wt% NaCl solution at 60°C with no inhibitor (✳), adding mixture inhibitor (1.875×10^{-5} mol/L PQ+1.875×10^{-5} mol/L QQ+1.25×10^{-5} mol/L TU) initially and measuring EIS after immersing for 90 minutes (curve 3), adding three-component inhibitor separately, labeled as $^1TU^2PQ^3QQ$ (○), $^1TQ^2QQ^3PQ$ (●),$^1PQ^2TU^3QQ$ (△), $^1PQ^2QQ^3TU$ (▲), $^1QQ^2TU^3PQ$ (◇) and $^1QQ^2PQ^3TU$ (◆), in which 1, 2, 3 represent the order of addition at t=0 min, 30 min, 60 min by fixed molar ratio and testing after 30, 60 and 90 minutes).

Figure 9(a-c) reveals three equivalent circuits, which can be fitted from the experimental data in the blank solution and with the addition of corrosion inhibitors. The equivalent circuit of Figure 9(a) can be fitted with the uninhibited solution or little inhibition such as single TU, PQ and $^1TU^2PQ$, containing the solution resistance (R_s), charge transfer resistance (R_{ct}), and constant phase element (CPE_{dl}) [31,32].
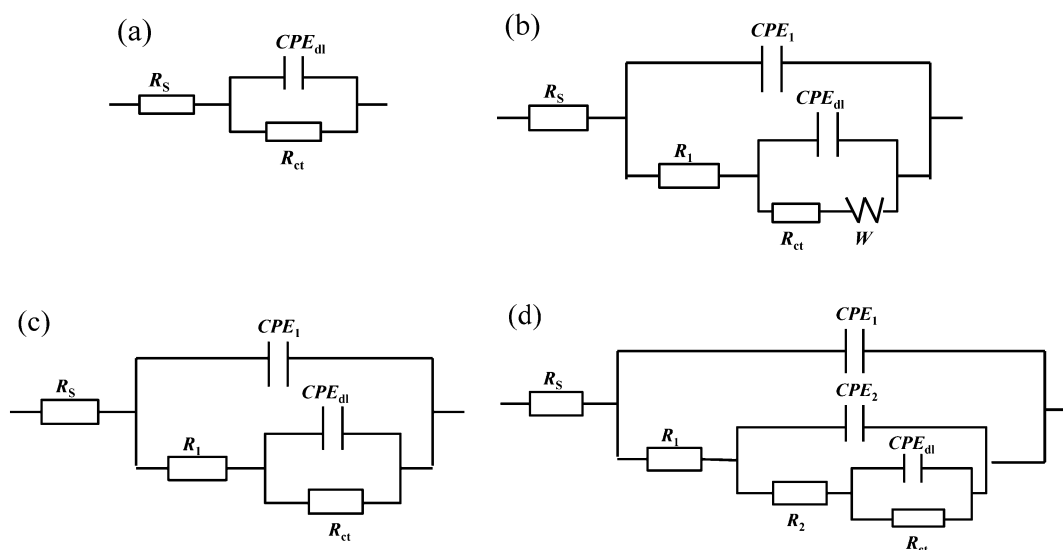
Figure 9. Different equivalent circuit diagrams (a-d) used to fit impedance spectrums.

Figure 9(b) is used to illustrate the simultaneous addition of three inhibitors at the beginning of immersion, where W represents the Warburg resistance. Figure 9(c) is used to fit the EIS plot of adding all inhibitors simultaneously after 90 minutes and the addition of two or three inhibitors in order. This

model indicates the existence of a more uniform protective film by the inhibitors on the metal surface, where R_f and CPE_f are the resistance and capacitance of the inhibitors film [33], respectively. Moreover, with the addition of inhibitors at the same time in the initial stage, the low frequency region of the Nyquist plot shows the feature of Warburg resistance (W), revealing that the corrosion process is under diffusion control [34]. The experimental data obtained after the three inhibitors are added in completely different orders, including ${}^1TU^2PQ^3QQ$, ${}^1TU^2QQ^3PQ$, ${}^1PQ^2TU^3QQ$ and ${}^1QQ^2TU^3PQ$ are fitted by the equivalent circuit in Figure 9(d). This circuit model represents the formation of porous bilayer inhibitor films due to the addition sequence of the inhibitors, in which R_1 and CPE_1, and R_2 and CPE_2 represent the resistance and capacitance of the outer and inner layers of the inhibitor films [35], respectively.

The relevant electrochemical parameters after fitting are shown in Table 2. As seen from Table 2, R_{ct} is increased and the diffusion process no longer occurs in the low-frequency region with the increase of time. This is due to the dynamic adsorption process of the inhibitors, which eventually forms a dense protective film on the metal surface. It is worth mentioning that the total resistance obtained for each addition is close to the value of the polarization resistance R_p obtained with the direct current polarization method [36]. On the other hand, the value of R_{ct} in this case has little difference from the lack of inhibitor when adding PQ, QQ and TU alone, respectively. It indicates that the one-component inhibitor has poor ability in forming a film on the metal surface, which is consistent with the polarization measurement results. By adding another corrosion inhibitor at t=30 min, the inhibition effect has been improved to some extent. For adding TU preferentially in the three-component inhibitor, the EIS patterns are completely different. The reason is that TU adsorbs preferentially on the metal surface, hindering the subsequent adsorption of PQ or QQ at the active site [37]. Larger molecules require cost more energy to replace TU or are directly adsorbed on the surface of TU to form bilayer film. However, due to that the formation of the layer by TU is not a dense film, the integrated inhibition efficiency is poor. From Table 2, the inner layer resistance (R_2) is greater than the outer layer resistance (R_1), which may be related to the dense degree of film formed by the inhibitors [35]. In addition, in the case of adding TU in the middle, such as ${}^1PQ^2TU^3QQ$ and ${}^1QQ^2TU^3PQ$, the obtained fitting results also have a great difference from the simultaneous addition. It suggests that the film of TU is not condense enough and protective. However, if TU is the last added inhibitor, such as ${}^1PQ^2QQ^3TU$ and ${}^1QQ^2PQ^3TU$, the total resistance is enlarged. It is close to the EIS plots of adding the mixture of inhibitors (three-component) preferentially. Therefore, it illustrates that these orders of addition are similar to the actual adsorption of adding the mixture of inhibitors at t=0 min.

Table 2. Electrochemical parameters of impedance spectra for carbon steel in CO_2-saturated 3.5 wt% NaCl solution in the absence and presence of different corrosion inhibitor at 60°C.

Inhibitor	R_s (Ω cm²)	R_1 (Ω cm²)	R_2 (Ω cm²)	R_{ct} (Ω cm²)	W ($s^{0.5}/\Omega$ cm²)	R_p (Ω cm²)
Blank	2.4	-	-	117.1	-	-
1	2.3	20.6	-	818.9	0.02	1174.0
2	2.3	21.3	-	926	0.02	1056.3
3	2.3	11.2	-	920.4	-	1055.6

TU	2.3	-	-	134.5	-	104.8
PQ	2.3	-	-	149.3	-	172.9
QQ	2.1	1.7	-	396.5	-	489.2
^{1}TU ^{2}PQ	2.3	-	-	161.0	-	143.0
^{1}TU ^{2}QQ	2.3	56.98	-	319.4	-	260.1
^{1}PQ ^{2}TU	2.2	107.8	-	92.2	-	171.0
^{1}PQ ^{2}QQ	2.4	21.8	-	577.2	-	762.6
^{1}QQ ^{2}TU	2.2	11.3	-	593.8	-	587.1
^{1}QQ ^{2}PQ	2.1	4.2	-	704.7	-	792.2
^{1}TU ^{2}PQ ^{3}QQ	2.2	1.2	19.0	361.9	-	321.3
^{1}TU ^{2}QQ ^{3}PQ	2.3	1.15	7.56	422.2	-	321.3
^{1}PQ ^{2}TU ^{3}QQ	2.3	32.1	607.8	135.0	-	644.6
^{1}PQ ^{2}QQ ^{3}TU	2.2	13.4	-	835.8	-	925.8
^{1}QQ ^{2}TU ^{3}PQ	2.4	3.4	18.4	695.1	-	642.7
^{1}QQ ^{2}PQ ^{3}TU	2.4	6.6	-	911.4	-	948.8

3.2.4. Synergistic mechanism

Three inhibitors (PQ, QQ and TU) with independent and synergistic effect with each other were evaluated. The molecular structure of the inhibitors and the synergistic effect of the inhibitors with different structures have a great influence on the inhibition efficiency. The three-component inhibitor PQ+QQ+TU (1.5:1.5:1) achieved a satisfactory corrosion inhibition efficiency. The adsorption order of the three-component inhibitor on the metal surface is found by electrochemical methods including linear polarization method and electrochemical impedance spectroscopy to monitor the transient process (in 3.2). The results show a similar adsorption sequence to the actual situation. The adsorption sequence of the three inhibitors on the Q235 surface can be illustrated by Figure 10. Several models of ultimate adsorption on the metal surface are proposed. It is shown that the adding sequence of inhibitors has pronounced influence on the model. Figure 10(a) shows the adsorption model of adding the three inhibitors in a fixed ratio at the same time and adding the inhibitors in the sequence of ^{1}QQ^{2}PQ^{3}TU or ^{1}PQ^{2}QQ^{3}TU. In this model, the big molecule, PQ or QQ, occupies the active vacancy at the metal surface. Afterwards, the small molecule TU fills in the vacancy to form a compact film. The quantum chemical calculations (in 3.4) also prove that QQ has the strongest reactivity. It might adsorb on the most suitable active sites preferentially than the other inhibitors. Figure 10(b) reveals the condition of adding TU first and then adding PQ and QQ in different order. In this model, TU adsorbs on the metal surface preferentially to form a bottom film. Later, the ring compounds adsorb on TU to form a crystal compound [37]. The crystal compound connects with the bottom TU film to construct a complex bilayer adsorption film on the metal surface. The TU molecules occupy most of the active sites at the interface. However, the bottom TU film is not strong enough to provide sufficient protection to the metal. This results in the relatively worse protection effects than adding other inhibitors preferentially. Figures 10(c) and (d) represent the circumstance of adding PQ or QQ preferentially and then TU. The inhibition efficiencies are better than adding TU preferentially but not as good as adding TU in the end. Similarly, it can be ascribed to the formation of the crystal compound by TU with the later added inhibitor. The existence

of TU in the middle can not offer sufficient protection to the substrate metal. The significant inhibition effect is based on forming a dense protective film on the metal surface.
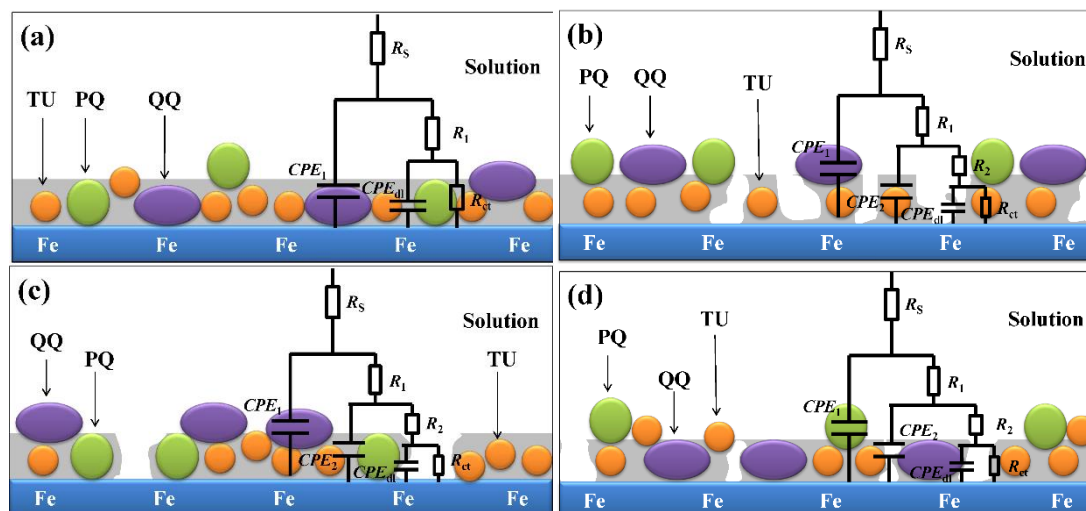
**Figure 10.** Adsorption models from different inhibitor adding orders.

3.3. XPS analysis

The XPS experiments were carried out to quantitatively and qualitatively analyze the formation of inhibitors on the metal surface. Figure 11 shows the wide-scan XPS spectrum of the sample after immersion in the CO_2-saturated 3.5 wt% NaCl solution with the addition of PQ, QQ, and TU (molar ratio of 1.5: 1.5: 1) at the same time for 90 minutes. As seen from Figure 11, there are elements of C, N, O, and Fe, in which the contents of C, O, and N are high and Fe is hardly detected. It indicates that the inhibitors form a dense molecular film on the metal surface. The detected nitrogen atom is from PQ, QQ, and TU. N 1s exists in the following two forms: one is the Fe-N adsorption bond (399.6 ± 0.1 eV) [13,38], which is mainly contributed by the pyridine, quinoline and the ammonium groups of quaternary ammonium salt, and another is C-N-H_2 (400.9 ± 0.3 eV) from thiourea [39–41].
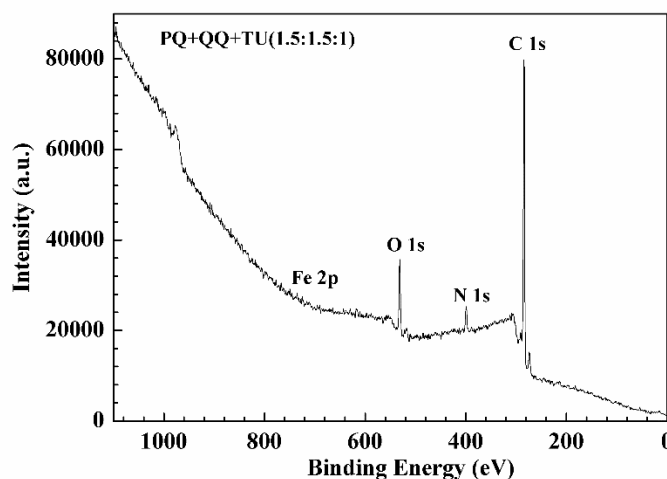
Figure 11. The wide-scan XPS spectrum for Q235 steel after immersed in CO_2-saturated 3.5 wt% NaCl solution with three-component inhibitor for 90 minutes at 60°C.

Figure 12(a) is the high-resolution spectrum of N 1s with the addition of three-component inhibitor simultaneously and immersion for 90 min. Figure 12(b) is adding inhibitors with the order of TU, PQ, and QQ at every 30 min and total immersion for 90 min. Figure 12(c) is and adding inhibitors with the order of QQ, PQ, and TU at every 30 minutes and total immersion for 90 min. The influence of different adding order of inhibitors on the film formation can be analyzed by calculating the nitrogen peak content ratio in the spectrum. Compared with the experimental results of the simultaneous addition, when TU is added at the beginning, TU will preferentially adsorb on active sites of the metal surface as much as possible. Moreover, the content of C-N-H_2 will be increased rapidly. In addition, due to the special nature of TU, the subsequent addition of PQ and QQ will be superimposed on the thiourea molecules to form a nondense bilayer membrane, so the content of Fe-N is reduced. However, the final results between adding inhibitors one by one and adding all at the beginning are quite different, This, sheds light that the time has a great impact for inhibitors to adsorb on the metal surface and the formation of inhibition films on the metal surface is quite rapid. So a qualitative analysis can be conducted by comparing the content ratios of the two forms of N 1s [42]. Table 3 shows the different peak area ratios of N 1s. Among them, the area ratio is 2.7 when adding the inhibitors at the same time. For the system of $^1TU^2PQ^3QQ$, it is 0.63, and for $^1QQ^2PQ^3TU$, it is 2.6. It is proved that the film for the order of $^1QQ^2PQ^3TU$ is similar as adding the three-component inhibitor simultaneously. The result is consistent with the electrochemical behavior.
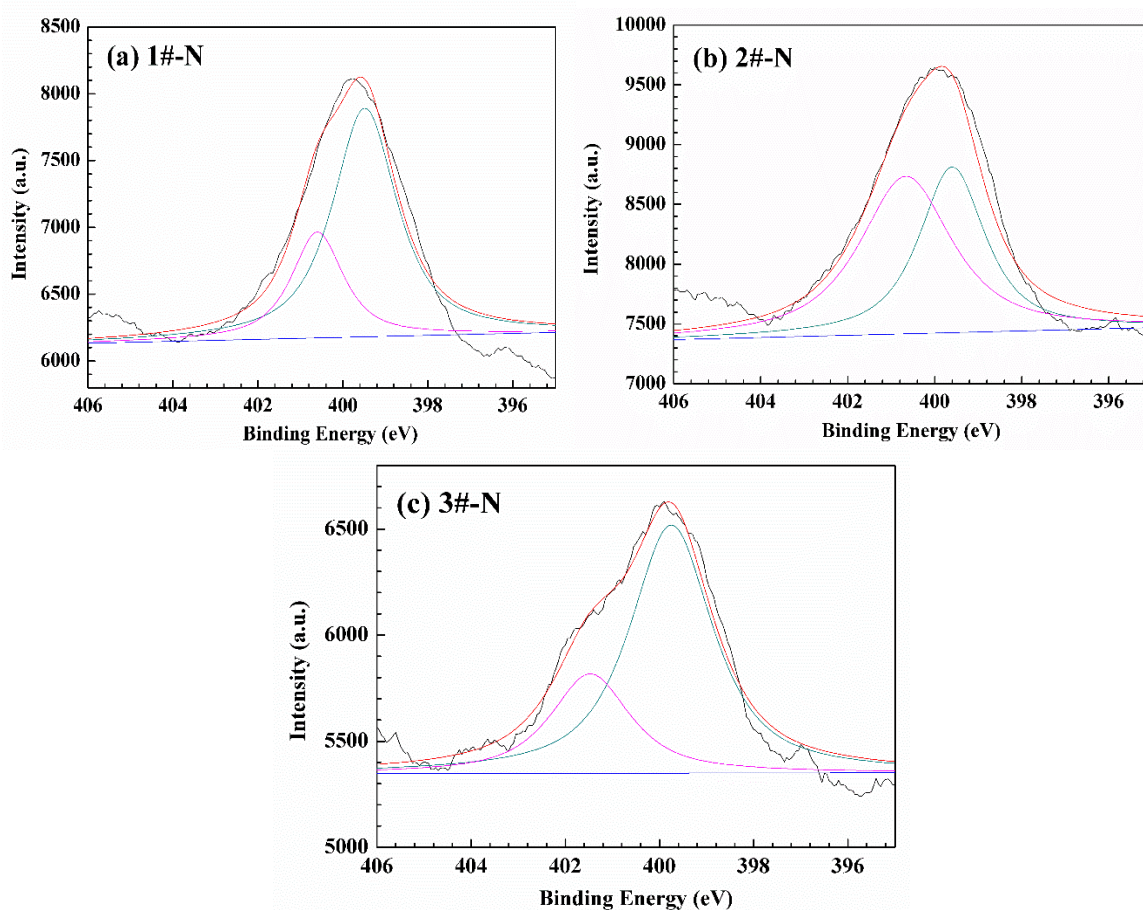

Figure 12. High-resolution XPS spectrum of N 1s for Q235 steel after immersed in CO_2-saturated 3.5 wt% NaCl solution at 60°C with (a) three-component inhibitor added simultaneously, (b) $^1TU^2PQ^3QQ$ and (c) $^1QQ^2PQ^3TU$.

Table 3. Parameters of XPS spectrum of N 1s from high-resolution for Q235 steel after immersed in CO_2-saturated 3.5 wt% NaCl solution containing different inhibitors at 60°C.

Inhibitor	N 1s peak type	N 1s position(eV)	N 1s peak area	Ratio of N 1s peak area
1#-N	Fe-N	399.5	4524.9	2.7
	C-N-H_2	400.6	1689.2	
2#-N	Fe-N	399.5	3080.8	0.63
	C-N-H_2	400.7	4908.4	
3#-N	Fe-N	399.7	3606.7	2.6
	C-N-H_2	401.2	1376.4	

3.4. Quantum chemical calculations

Quantum chemical calculation is a powerful method to prove the correlation between the structure and inhibition performance in theory. Through geometrical optimization and investigating frontier molecular orbitals, the parameters including highest occupied molecular orbital (HOMO) and lowest unoccupied molecular orbital (LUMO) of PQ, QQ and TU, have been obtained. These can predict the ability of the adsorption of inhibitors on the metal surface.

$E_{HOMO}= -8.123$ $E_{LUMO}= -0.002$

$E_{HOMO}= -7.318$ $E_{LUMO}= -0.754$

$E_{HOMO}= -7.255$ $E_{LUMO}= -0.110$
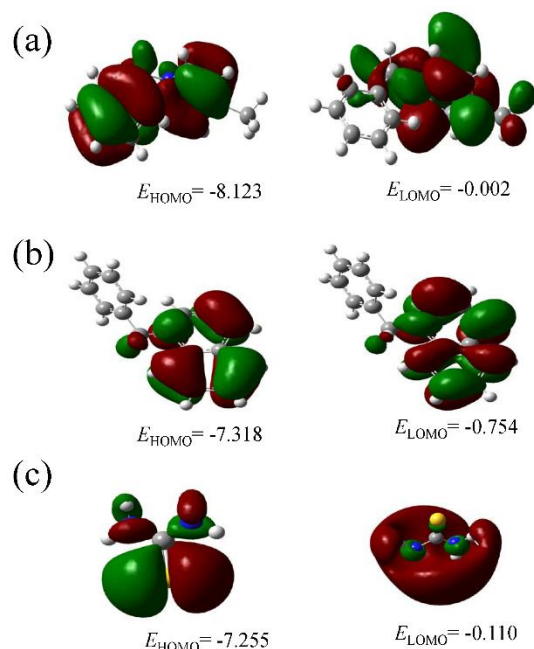
Figure 13. Schematic representation of HOMO and LUMO molecular orbital of (a) PQ, (b) QQ and (c) TU (Color code: N, blue; S, yellow; C, gray; H, white).

The higher the E_{HOMO}, which is associated with the electron donating ability of the molecule, the easier it is for the electrons of the inhibitors to be donated to the vacant d-orbitals of the metal atoms. The value of E_{LUMO} indicates the ability of accepting electrons, and the lower the value, the more probable of accepting electrons [26]. In addition, the energy difference between the lowest empty orbital and the highest occupied orbital ΔE ($E_{LUMO} - E_{HOMO}$) is an important index of molecular stability; the

greater the difference, the stronger the stability. In contrast, the lower value of ΔE indicates a high reaction activity and better inhibition efficiency [43]. From Figure 13, it is evident that both TU and QQ have a strong electron donating ability to be adsorbed on the surface, due to the lone pairs of sulfur atom and nitrogen atom or the π-electrons of the pyridine ring and benzene ring. However, QQ would accept electrons better than TU or PQ.

Table 4. Calculated quantum chemical properties for PQ, QQ and TU.

Inhibitor	E_{HOMO}	E_{LUMO}	ΔE	$IE\%$
PQ	-8.123	-0.002	8.121	-19.7
QQ	-7.318	-0.754	6.564	51.2
TU	-7.255	-0.110	7.146	15.7

The related parameters are shown in Table 4. The ΔE value obeys the order: QQ < TU < PQ. It can be seen that QQ has the strongest reactivity. It may adsorb on the metal surface first, which is in accordance with the result of OCP in the electrochemical experiments. Moreover, this result is consistent with the experiments of the inhibition efficiency of the one-component inhibitor.

4. CONCLUSIONS

1 The polarization curves proved that there are remarkable synergistic effects between PQ, QQ and TU. The three inhibitors exhibit different performance when used alone. Apparent synergistic effects occur in the bicomponent inhibitors and the best inhibition efficiency is observed for PQ+QQ (1:1). The three-component inhibitor PQ+QQ+TU (1.5:1.5:1) displays the best performance overall, indicating the best synergistic effect in all inhibitors.

2 The three inhibitors, PQ, QQ and TU, have different abilities in film forming at the Q235 surface, regardless of whether they are used alone or in synergy. It reveals that the influence orders of the three inhibitors are as follows: QQ > PQ > TU. It indicates that the film of TU on the metal surface is not very protective. In contrast, PQ and QQ can form a more effective film on the metal surface.

3 It is demonstrated that the different addition sequence of the three inhibitors has a significant influence on the synergistic effect. This is due to the competitive adsorption and film forming processes of inhibitors on the metal surface. The values of R_p, from the linear polarization, are very close to the total resistance in the impedance. Regardless of whether single TU is added preferentially or added in the middle, no good synergistic effect could be achieved. On the other hand, the sequence of ^{1}QQ^{2}PQ^{3}TU fits most closely with the actual situation.

4 The composition of the film by the inhibitors was analyzed by XPS. It reveals that a dense molecular film is formed by adding the three-component inhibitor at the beginning of immersion. The effect of the addition order on the film formation is consistent with the electrochemical behavior.

5 The mechanism of synergistic effects within the three-component inhibitor is proposed. QQ and PQ preferentially adsorb on the active sites. Moreover, the small molecules TU fill into the vacancy to achieve the optimal film. The energy calculations of PQ, QQ and TU by quantum computational chemistry also reveal that QQ has a greater thermodynamic propensity to adsorb on the metal surface than PQ, due to the influence of the benzene ring structure. The results further demonstrate that the three inhibitor molecules form a denser inhibition film with an optimal order.

References

1. S. Nešić, *Corros. Sci.*, 49 (2007) 4308–4338.
2. A.Q. Liu, C. Bian, Z.M. Wang, X. Han, J. Zhang, *Corros. Sci.*, 134 (2018) 149–161.
3. M.B. Kermani, A. Morshed, *Corrosion,* 59 (2003) 659–683.
4. C. G., A. F., *Dev. Corros. Prot.*, (2014).
5. D.A. López, S.N. Simison, S.R. De Sánchez, *Corros. Sci.,* 47 (2005) 735–755.
6. L.D. Paolinelli, T. Pérez, S.N. Simison, *Corros. Sci.*, 50 (2008) 2456–2464.
7. C. Verma, L.O. Olasunkanmi, E.E. Ebenso, M.A. Quraishi, *J. Mol. Liq.*, 251 (2018) 100–118.
8. V. Jovancicevic, P. Prince, S. Ramachandran, *Corros. -Houst. Tx-.*, 55 (1999) 449–455.
9. G. Zhang, C. Chen, M. Lu, C. Chai, Y. Wu, Mater. *Chem. Phys.*, 105 (2007) 331–340.
10. B.M. Mistry, S.K. Sahoo, S. Jauhari, *J. Electroanal. Chem.*, 704 (2013) 118–129.
11. D. Zhang, L. Li, L. Cao, N. Yang, C. Huang, *Corros. Sci.*, 43 (2001) 1627–1636.
12. G. Achary, H.P. Sachin, Y.A. Naik, T. V. Venkatesha, *Mater. Chem. Phys.*, 107 (2008) 44–50.
13. J. Zhao, H. Duan, R. Jiang, *Corros. Sci.*, 91 (2015) 108–119.
14. S.A.A. El-Maksoud, A.S. Fouda, *Mater. Chem. Phys.*, 93 (2005) 84–90.
15. H. Ma, S. Chen, Z. Liu, Y. Sun, *J. Mol. Struct. Theochem.*, 774 (2006) 19–22.
16. M. Lashkari, M.R. Arshadi, *Chem. Phys.*, 299 (2004) 131–137.
17. K.R. Ansari, M.A. Quraishi, A. Singh, *J. Ind. Eng. Chem.*, 25 (2015) 89–98.
18. Y. Xiao-Ci, Z. Hong, L. Ming-Dao, R. Hong-Xuan, Y. Lu-An, *Corros. Sci.,* 42 (2000) 645–653.
19. P.C. Okafor, Y. Zheng, *Corros. Sci.*, 51 (2009) 850–859.
20. J. Tang, *Int. J. Electrochem. Sci.*, 13 (2018) 3625–3642.
21. J. Zhao, G. Chen, *Electrochim. Acta*, 69 (2012) 247–255.
22. R. Fuchs-Godec, M.G. Pavlović, *Corros. Sci.,* 58 (2012) 192–201.
23. H. Wang, J. Tang, J. Xie, *Int. J. Electrochem. Sci.*, 12 (2017) 11017–11029.
24. N. M'hiri, D. Veys-Renaux, E. Rocca, I. Ioannou, N.M. Boudhrioua, M. Ghoul, *Corros. Sci.*, 102 (2016) 55–62.
25. D. Huang, J. Hu, G.L. Song, X. Guo, *Electrochim. Acta*, 56 (2011) 10166–10178.
26. G. Gece, *Corros. Sci.*, 50 (2008) 2981–2992.
27. S. Ghareba, S. Omanovic, *Electrochim. Acta*, 56 (2011) 3890–3898.
28. S. Javadian, A. Yousefi, J. Neshati, *Appl. Surf. Sci.*, 285 (2013) 674–681.
29. S.S. Abdel, O.A. Hazzazi, M.A. Amin, K.F. Khaled, *Corros. Sci.*, 50 (2008) 2258–2271.

30. R. Yildiz, *Corros. Sci*., 90 (2015) 544–553.
31. C.N. Cao, *Electrochim. Acta*, 35 (1990) 837–844.
32. B. Hirschorn, M.E. Orazem, B. Tribollet, V. Vivier, I. Frateur, M. Musiani, *Electrochim. Acta*, 55 (2010) 6218–6227.
33. C. Georges, E. Rocca, P. Steinmetz, 53 (2008) 4839–4845.
34. H. Tian, W. Li, B. Hou, D. Wang, *Corros. Sci*., 117 (2017).
35. M.P. Desimone, G. Grundmeier, G. Gordillo, S.N. Simison, *Electrochim. Acta,* 56 (2011) 2990–2998.
36. A. Popova, M. Christov, A. Vasilev, *Corros. Sci*., 94 (2015) 70–78.
37. J.M. Zhao, H.X. Liu, D.I. Wei, Y. Zuo, *Electrochemistry,* 10 (2004) 440–445.
38. K. Hu, J. Zhuang, J. Ding, Z. Ma, F. Wang, X. Zeng, *Corros. Sci.,* 125 (2017).
39. G.W. Nelson, M. Perry, S.M. He, D.L. Zechel, J.H. Horton, *Colloids Surfaces B Biointerfaces*, 78 (2010) 61–68.
40. L. Fertier, M. Rolland, T. Thami, M. Persin, C. Zimmermann, J.L. Lachaud, D. Rebière, C. Déjous, E. Bêche, M. Cretin, *Mater. Sci. Eng.* C., 29 (2009) 823–830.
41. P. Singh, V. Srivastava, M.A. Quraishi, *J. Mol. Liq.*, 216 (2016) 164–173.
42. C. Zhang, H. Duan, J. Zhao, *Corros. Sci*., 112 (2016) 160–169.
43. I.B. Obot, D.D. Macdonald, Z.M. Gasem, *Corros. Sci.*, 99 (2015) 1–30.